Automated Muscle Segmentation from Dynamic Computed Tomographic Angiography Images for Diagnosis of Peripheral Arterial Occlusive Disease

ZEHONG LIN [1], HE XU[1], AND DAMING ZHANG[2]

[1]College of Mechanical and Electrical Engineering, Harbin Engineering University, Harbin 150001, China
[2]Peking Union Medical College Hospital, Chinese Academy of Medical Sciences, Peking Union Medical College, Beijing 100730, China

Corresponding author: He Xu (dloinng@163.com)

ABSTRACT The purpose of this study was to quantitatively evaluating lower leg muscle ischemia measured from dynamic computed tomographic angiography (dyn-CTA) for patients with peripheral arterial occlusive disease (PAOD). A total of 35 patients with known PAOD underwent a dyn-CTA of the lower leg first with 70 kV tube voltage and 30 mL iodinated contrast media. Five minutes later, a standard CTA (s-CTA) of the peripheral runoff from the diaphragm to the toes was scanned. For each of four lower leg artery segments, a runoff score was given by a radiologist according to s-CTA images as a reference standard. The muscle enhancement measured from the dyn-CTA was analyzed by automated muscle segmentation using curve-based Fuzzy C-means (CBFCM) algorithms with three classes for bone, two classes for muscle and one class for fat and background. The muscle enhancement ratio (MER) was calculated for (i) higher enhanced area over total area; and (ii) corresponding average signal value at higher enhanced are over total area. Lower extremities were diagnosed as a normal group (n = 22) with each vessel segment score ≤ 1 and runoff score ≤ 7, and otherwise as an ischemia group (n = 48). The MER for the ischemia group was significantly different ($p < 0.05$) than the normal group. There were weak correlations ($|r| = 0.47$, $p < 0.05$) between runoff scores and the MER values. The receiver operating characteristics (ROC) analysis between the two groups had area under the curve of 0.71-0.73. Our study demonstrated that CBFCM could be used for automated muscle segmentation from the dyn-CTA images for qualitatively evaluation of lower leg muscle ischemia.

INDEX TERMS Curve-based Fuzzy C-means, dynamic computed tomographic angiography, lower leg muscle ischemia, peripheral arterial occlusive disease, standard computed tomographic angiography.

I. INTRODUCTION

Lower leg peripheral arterial occlusive disease (PAOD) prevalence and incidence are both sharply age-related and rising >10% among patients in their 60s and 70s [1]. The prevalence in high income country at age 85–89 years was ~18% in women and ~19% in men. Globally, 202 million people were living with peripheral artery disease in 2010 [2]. Lower leg ischemia has a direct adverse effect on calf skeletal muscle area [3], [4]. Patients with PAOD not only have their

The associate editor coordinating the review of this manuscript and approving it for publication was Byung-Gyu Kim [ID].

physical functions most affected, but often have concomitant coronary and cerebral artery disease [5], [6].

The PAOD has often been diagnosed with noninvasive angiography, such as using computed tomography (CTA), magnetic resonance angiography (MRA), as well as with duplex ultrasonography (US) [7], [8]. Both CTA and MRA provide a high resolution 3-dimensional road map of the peripheral arterial tree in patients for visualization of the vasculature [9]. However, the diagnostic value is only promising for large caliber arteries (from the aorta to the popliteal artery). For the arteries beneath knees, there were studies demonstrated that dynamic CTA (dyn-CTA) increased

diagnostic confidence for the assessment of the presence and degree of arterial stenosis than standard CTA (s-CTA) [10], [11]. The dyn-CTA is very useful for identification of specific calcified vessels and can distinguish between calcified and occluded vessels [12]. However, up to now, almost all diagnosis of PAOD is qualitative based on vascular anatomical appearance and there is lack of quantitative parameters for evaluating muscle ischemia.

MRI and CT images are also commonly used for the study of skeletal muscle distribution and quantification in different body regions with relevant clinical impact [13]. There are many automated tissue segmentation methods to find ''hard partition'' of a given dataset based on certain criteria that evaluate the goodness of partition, such as histogram-based, region-based, edge-based, model-based, watershed methods [14]–[16]. In contrast, the Fuzzy C-Means algorithm is an unsupervised fuzzy clustering algorithm used in tissue segmentation [17], such as liver [18]–[20], brain [21], [22], breast [23]–[25] and head and neck cancer [26]. All above studies using Fuzzy C-Means mainly focused on identification of cancer. To the best of our knowledge, there is no study using Fuzzy C-Means on dyn-CTA images for automated muscle segmentation for diagnosis of PAOD to evaluate muscle ischemia.

In this study, the curve-based Fuzzy C-means (CBFCM) algorithm was used to segment the lower leg muscle enhancement measured from the dyn-CTA to quantitatively evaluate muscle ischemia. The dyn-CTA and s-CTA were performed using 70 kV tube voltage and low dose of iodinated contrast media (CM) to significantly reduce the radiation dose [27]–[29]. The segmented muscle area and corresponding average signal over the muscle area at the last time point of the dyn-CTA were calculated and used for calculating the muscle enhancement ratios (MER).

II. MATERIALS AND METHODS
A. PATIENTS AND DATA ACQUISITION
This study was approved by the Institutional Review Board at Peking Union Medical College Hospital, Beijing China. Patients were enrolled from November 2015 to March 2016. Informed consent was obtained from all patients prior to any study procedures. A total of 35 patients (average age = 66.6±11.7 years old; 11 female, 24 male) with known PAOD were enrolled in this study. Based on runoff score obtained from diagnosis of s-CTA images, all 35 patients with 70 lower extremities were divided into a normal group and an abnormal group with ischemia.

All scans were performed on a third generation dual source CT system (Somatom Definition Force; Siemens Healthcare, Forchheim, Germany) with the capability of dynamic imaging by using a shuttle mode. The dyn-CTA scan was immediately started as soon as the arteries were enhanced at the premonitory position, where it was 15 cm above the superior border of the scan range of the dyn-CTA. The scan was performed from the knees to the toes with 150 slices. Five minutes later, the s-CTA of the peripheral runoff from

TABLE 1. Detailed CTA scan parameters.

Parameter	dynamic CTA	standard CTA
scan range	45 cm	diaphragm to toes
tube voltage	70 kV	70 kV
tube current	80 mAs	322 mAs
collimation	2×64×0.6 mm	2×64×0.6 mm
contrast media	30 mL; Iopromide, 370 mgI/mL; Bayer HealthCare	50 mL; Iopromide, 370 mgI/mL; Bayer HealthCare
flow rate	4.0 mL/s	2.5 mL/s
saline flush	50 mL 4.0 mL/s	40 mL 2.5 mL/s
pitch	--	0.6
rotation time	--	0.25 s
images thickness	5 mm	5 mm
increment	3 mm	3 mm
scan time	30 s (5 phases with 2.5 s and 4 phases with 5 s)	--

the diaphragm to the toes was performed [11], [13]. The s-CTA scans were triggered with a bolus tracking technique. A region of interest (ROI) was placed on the healthy popliteal artery, and the s-CTA scan automatically initiated after 6 s when a threshold of 100 Hounsfield Unit (HU) was achieved. All the dyn-CTA and s-CTA scan parameters are given in Table 1.

For estimating the CTA radiation dose, the volume CT dose index (CTDIvol) and the dose length product (DLP) of each patient were recorded. The conversion coefficients k for effective dose (ED) was adopted from the study of the estimation ED of lower legs by Saltybaeva [30].

For each of four lower leg artery segments, stenosis percentage and occlusion length were evaluated and a score was given by a vascular imaging radiologist (DZ, 8-year experience) according to the s-CTA diagnostic outcome. The score ranges from 0 to 19, with a higher score indicating more severe disease. The evaluation criterion is given in Table 2. The score for the popliteal artery is multiplied by 3 according to existing standard and 1 is added before sum all 4 vessel scores together as runoff score for a lower leg [31].

TABLE 2. Evaluation criterion.

Score assigned	Degree of vessel stenosis
0	with <20% stenosis
1	with 21-49% stenosis
2	With 50-99% stenosis
2.5	a vascular occlusion less than half its length
3	an occlusion greater than half of the length

B. TISSUE SEGMENTATION
Tissue segmentation was achieved by applying curve-based Fuzzy C-means (CBFCM) clustering for the dyn-CTA data. The CBFCM algorithm is based on tissue time attenuation curves, while the traditional FCM algorithm is mainly based on the image pixel values. All the data analysis was performed using MATLAB (MathWorks, Natick, MA) with in-house software. The dyn-CTA data were analyzed by a medical physicist, who was blinded to the patients' diagnostic results.

Prior to applying the CBFCM to the dyn-CTA data, the patient bed needs to be removed from the source data to avoid confusion with tissue segmentation. Since there was a big gap between patient bed and legs in CT image, the bed was easily isolated and its image was replaced by CT value of air. Then the 20th, 30th, and 40th axial slices were used for tissue segmentation using the CBFCM algorithm, because these slices were at the larger section of the legs with clear blood vessels and muscle region. Based on some trial analysis, the number of classes was set to be six, including three classes for bone, two classes for muscle and one class for fat and the background.

For each pixel, there was a time attenuation curve (TAC) measured from the dyn-CTA data. For each slice, there was a data set $S = \{s_i, i = 1, 2, \ldots, N\}$, where $N (= 512 \times 512)$ is total number of pixels, $s_i = (TAC_{i1}, TAC_{i2}, \ldots, TAC_{i,T})$ is a vector containing CT value of the ith pixel at time point t (TAC_{it}), and $T (= 9)$ is total number of time points in the dyn-CTA. In this research, we attempted to partition the dataset S into $c (= 6)$ classes.

The detailed CBFCM algorithm was published by Chen *et al.* in 2006 [25]. In brief, the prototypic curves corresponding to the c classes were represented by a $c \times T$ matrix V, with the kth ($k = 1, 2, ..., c$) row is a T-dimensional vector representing the prototypic curve of the kth class. The partition of the data set is represented by a $c \times N$ matrix U, with each element represents the ith data point s_i to the kth class. In the calculations, matrix V was randomly initialized, and then U and V were obtained through an iterative process. The convergence criterion of the iteration was that the Euclidean distance between the current prototype matrix and the prototype matrix in the previous iteration was less than some user-specified number ε, i.e., $||V_{new} - V_{old}|| < \varepsilon$. The flowchart of the segmentation steps is shown in Fig. 1.

C. MUSCLE ENHANCEMENT

Total automated muscle segmentation area was compared with manually segmented muscle area as verification of accuracy. The manual segmented muscle was achieved by using threshold value to remove bone first, and then manually traced around edge of muscle regions.

For each slice, the muscle enhancement ratio (MER) based on area (MER$_{area}$) was calculated by higher enhanced muscle area over total muscle area, i.e.,

$$MER_{Area} = \frac{Higher\ enhanced\ muscle\ area}{Total\ muscle\ area}. \quad (1)$$

In addition, the MER based on average signal value (MER$_{Signal}$) over corresponding muscle areas was also calculated as follows:

$$MER_{Signal} = \frac{Average\ signal\ over\ higher\ enhanced\ muscle\ area}{Average\ signal\ over\ whole\ muscle\ area}. \quad (2)$$
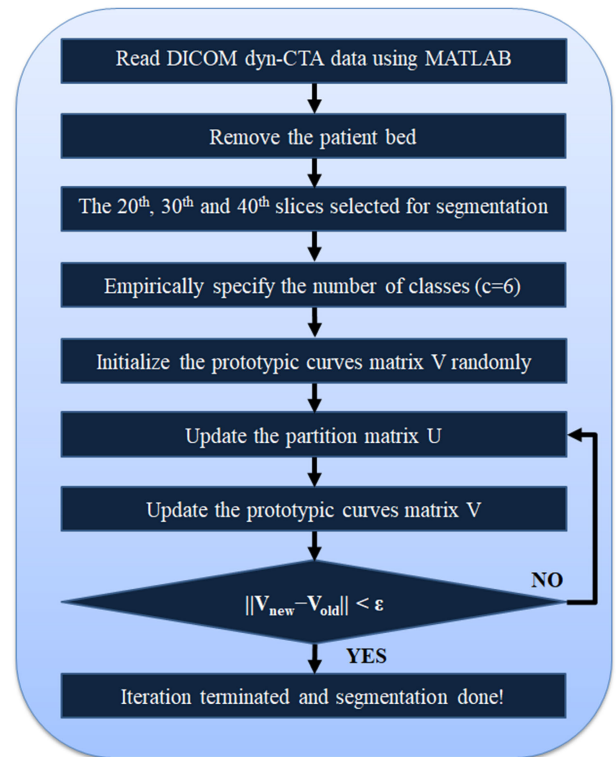

FIGURE 1. The flowchart of the segmentation steps used in the CBFCM.

Finally, averaged MER between three slices was used as a final MER value and compared between normal group and abnormal group with ischemia.

All statistical analyses were performed using the Statistical Package for Social Sciences, version 19.0 (SPPS Inc., Chicago, IL, USA). For calculated MER parameters, Student t-tests were performed to exam whether there were significant differences between the normal and abnormal group with ischemia.

The Pearson correlation coefficients were calculated between runoff scores and MER parameters. Receiver operating characteristics (ROC) analysis was performed to evaluate whether MER parameters could be used for classification of normal lower leg vs. abnormal lower leg with muscle ischemia. A p-value less than 0.05 was considered significant.

III. RESULTS

For all 35 patients (Fontaine stage I, n=5; Fontaine stage II, n=21; Fontaine stage III, n=3; Fontaine stage IV, n=5, one for suspicious arterial aneurysm), the mean body mass index was 22.9 ± 3.0 kg/m^2 (range, 15.8 - 30.5 kg/m^2). Lower extremities were diagnosed as a normal group (n = 22) with each vessel segment score ≤ 1 and runoff score ≤ 7, and otherwise as an ischemia group (n = 48). The mean CTDIvol and DLP were 1.6 ± 0.3 mGy and 204.7 ± 45.2 mGy×cm for the s-CTA, and 9.1 ± 0.0 mGy and 396.9 ± 0.1 mGy×cm for dyn-CTA. The effective radiation dose of the combination
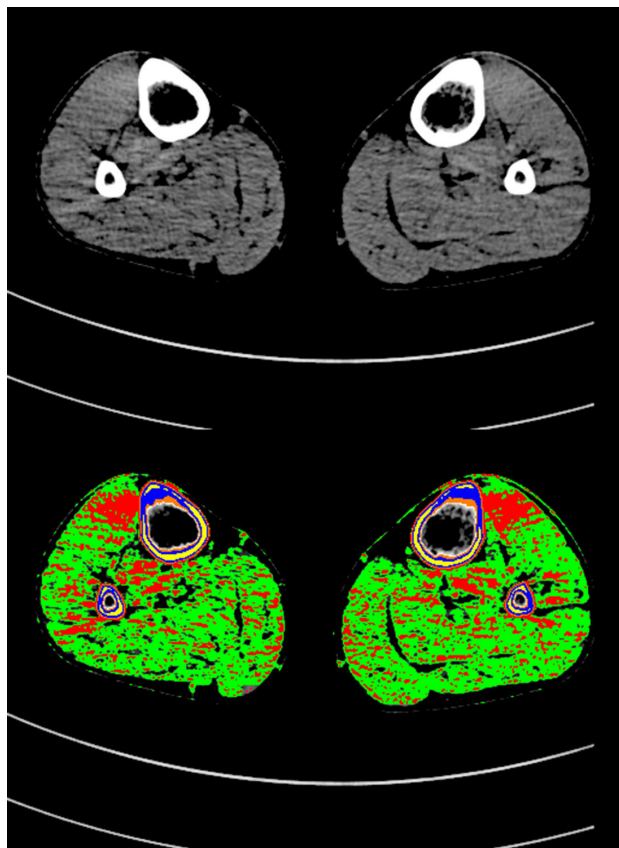
FIGURE 2. An axial slice of lower legs dyn-CTA image for 37 year old male patient with known normal (at right) and ischemia (at left). Top gray image is the 30th slice of the dyn-CTA at the last time point. Bottom is the corresponding segmentation results obtained from the CBFCM superimposed over gray image. The red and green colors represent higher and lower muscle enhancement region, respectively. The two curve lines at the bottom are the patient bed.
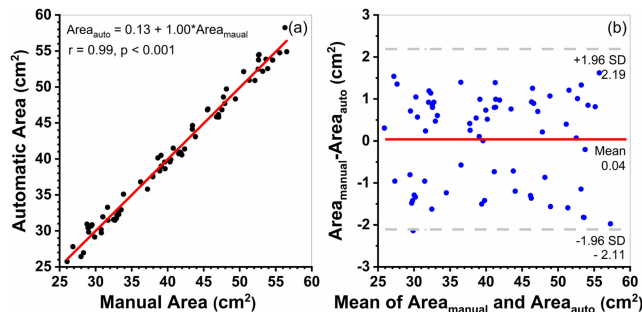

FIGURE 3. (a) The scatter plot of muscle area calculated between manual segmented muscle area and the CBFCM automated segmented muscle area. The red line is linear correlation that fits the data. (b) The corresponding Bland-Altman plot for the manual and automated segmented muscle area. The solid red line represents the mean difference and the dashed lines represent the lower and upper limits of agreement, defined by a range of $\pm 1.96*SD$ (95% confidence interval) around the mean.
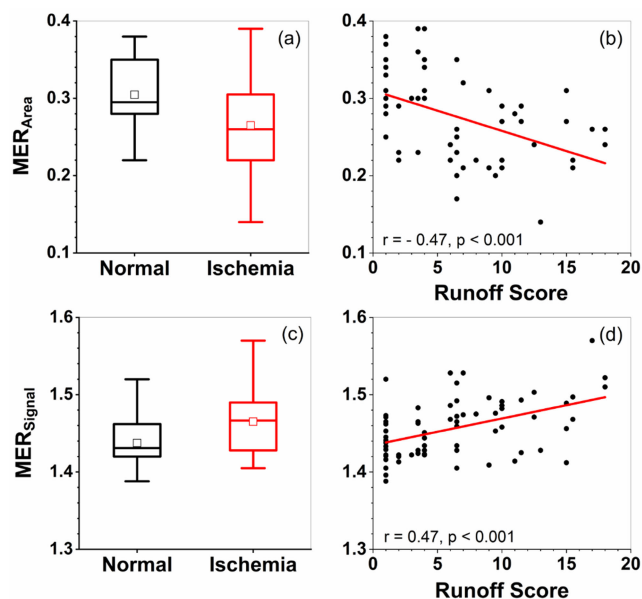

FIGURE 4. (a) The boxplot of the MER_{area} for normal (black) and ischemia (red) lower legs. (b) The scatter plots between runoff scores and the MER_{area}. (c) The boxplot of the MER_{signal} for normal (black) and ischemia (red) lower legs. (d) The scatter plots between runoff scores and the MER_{signal}. The square ($\square$) indicates mean of the data. The red line is linear correlation.

protocol with dyn-CTA and s-CTA was 2.0 ± 0.2 mSv and 1.0 ± 0.2 mSv, respectively.

Figure 2 shows (top) the 30th axial slice of dyn-CTA gray image at the last time point for a patient with asymmetric lower leg arterial stenosis, and (bottom) corresponding automated segmentation results obtained from the CBFCM: three classes for bone (represented by yellow, orange, and blue), two classes for muscle (higher (red) and lower (green) enhancement) and one class for fat and the background (black).

Figure 3 (a) shows a scatterplot between manual segmented muscle areas and the CBFCM automated segmented muscle area obtained from the 30th slice for all 70 legs. There was a strong correlation (r = 0.99) between manually and automatically segmented muscle areas. The reasons selected the 30th slice as an example because it was the largest section in the calf so that manually traced muscle area had less error. The corresponding Bland-Altman plot shows good agreement between the two area measurements (Figure 3 (b)) with bias of 0.04 cm^2 and limits of agreement between -2.11 to 2.19 cm^2.

Figure 4 (a) shows boxplot of the MER_{area} for both normal and ischemia groups. On average, the MER_{area} for the ischemia group was significantly lower (p < 0.05) than the normal group. There was a weak negative correlation (r = -0.47, p < 0.05) between runoff scores and the MER_{area} (Fig. 4 (b)). Figure 4 (c) shows boxplot of MER_{signal} for both normal and ischemia groups. On average, the MER_{signal} for the ischemia group was significantly higher (p < 0.05) than the normal group. There was a weak positive correlations (r = 0.47, p < 0.05) between runoff scores and the MER_{signal} (Fig. 4 (d)).

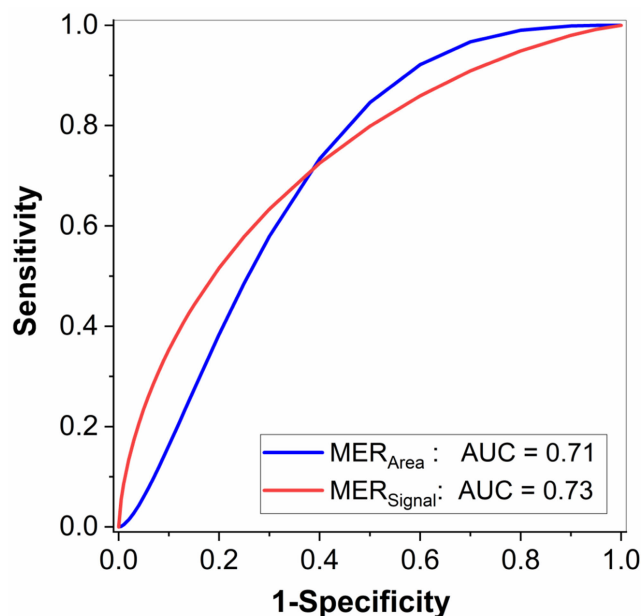Finally, Fig. 5 shows receiver operating characteristics (ROC) analysis results for the parameters MER_{area} and

FIGURE 5. The receiver operating characteristics (ROC) analysis results between normal and ischemia lower legs for the parameters MER_{area} and MER_{signal}.

MER_{signal} with the area under the curve (AUC) of 0.71 (blue line) and 0.73 (red line), respectively. It was demonstrated that there is fair diagnostic accuracy for the MER based on runoff scores as the reference standard. Moreover, combining parameters MER_{area} and MER_{signal} using logistic regression analysis could increase AUC to 0.75.

IV. DISCUSSION

The lower leg muscle enhancement measured by the dyn-CTA was quantitatively evaluated using the CBFCM algorithm for muscle segmentation. Our study demonstrated the feasibility of evaluating lower leg muscle ischemia based on automated muscle segmentation. The MER_{area} and MER_{signal} calculated from enhanced muscle area could be used as quantitative assessment for assisting the diagnosis of PAOD.

Newer CT scanners provide dynamic imaging range up to 60 cm in length, which is favorable for the dynamic multiphasic lower legs angiography [12]. The low tube voltage (70 kV) was proven to be feasible in CTA to reduce the radiation dose, as well as lower the CM volume to more than half [28], [29], [32]. Our study further demonstrated the feasibility of the protocol with low radiation dose (ED = 2.0±0.2 mSv), low iodinated contrast media (30 mL for dyn-CTA and 50 mL for s-CTA) as well as low tube voltage (70 kV) could be used in clinic for diagnosis of PAOD.

Previous studies of dyn-CTA were mainly on vascular morphology for better illustrate lumen stenosis of arteries. There was a lack of quantitative assessment for lower leg muscle ischemia. The vascular stenosis status may be not equal to the severity of lower leg muscle ischemia for several reasons [33]. First, the judgment of vascular stenosis relies on subjective evaluation, which is easily influenced by

human factors. Second, the vascular diameter (2 - 3 mm) is very thin for lower legs, which makes hard to determine stenosis from mild to severe, especially for severe stenosis and occlusion. Third, there were some side branches of blood vessels that developed for some patients, making it even hard to diagnosis stenosis accurately [34]. Therefore, our study could assist diagnosis in the clinic to provide quantitative measurement of muscle ischemia to some extent.

There are several limitations to this study. First, total iodinated contrast media (80 mL) used in this study is even less than normal s-CTA alone (90 mL). Therefore, the amount of contrast media could be slightly increased to get better muscle enhancement in the future study. Second, the dyn-CTA did not follow contrast media long enough to clearly shown contrast media uptake and washout in muscle. Third, our quantitative measurement was only compared with the runoff score, but did not compare with the gold standard digital subtraction angiography (DSA). This is because patients with mild muscle ischemia did not require an invasive examination. Fourth, the number of clusters used in the CBFCM was setup to six, which may not be proper for the other section of the leg. A more flexible number of clusters should be used in the future with artificial intelligent to better segment muscle enhancement.

In conclusion, the CBFCM could be used for automated muscle segmentation to quantitative evaluate tissue enhancement measured by the dyn-CTA. More studies are needed with a larger number of patients to establish reliable parameters to predict muscle ischemia in order to assist clinical diagnosis.

REFERENCES

[1] M. H. Criqui and V. Aboyans, "Epidemiology of peripheral artery disease," *Circulat. Res.*, vol. 116, no. 9, pp. 1509–1526, Apr. 2015.

[2] F. G. R. Fowkes, D. Rudan, I. Rudan, V. Aboyans, J. O. Denenberg, P. M. M. McDermott, P. P. E. Norman, U. K. A. Sampson, L. J. Williams, G. A. Mensah, and M. H. Criqui, "Comparison of global estimates of prevalence and risk factors for peripheral artery disease in 2000 and 2010: A systematic review and analysis," *Lancet*, vol. 382, no. 9901, pp. 1329–1340, Oct. 2013.

[3] R. Tanaka, K. Yoshioka, H. Takagi, J. D. Schuijf, and K. Arakita, "Novel developments in non-invasive imaging of peripheral arterial disease with CT: Experience with state-of-the-art, ultra-high-resolution CT and subtraction imaging," *Clin. Radiol.*, vol. 74, no. 1, pp. 51–58, Jan. 2019.

[4] M. M. McDermott, F. Hoff, L. Ferrucci, W. H. Pearce, J. M. Guralnik, L. Tian, K. Liu, J. R. Schneider, L. Sharma, J. Tan, and M. H. Criqui, "Lower extremity ischemia, calf skeletal muscle characteristics, and functional impairment in peripheral arterial disease," *J. Amer. Geriatrics Soc.*, vol. 55, no. 3, pp. 400–406, Mar. 2007.

[5] D. L. Bhatt, P. G. Steg, and M. Ohman, "International prevalence, recognition, and treatment of cardiovascular risk factors in outpatients with atherothrombosis," *JAMA*, vol. 295, no. 2, pp. 180–189, Jan. 2006.

[6] R. S. Dieter, W. W. Chu, J. P. Pacanowski, P. E. McBride, and T. E. Tanke, "The significance of lower extremity peripheral arterial disease," *Clin. Cardiol.*, vol. 25, no. 1, pp. 3–10, Jan. 2002.

[7] P. Riffel, H. Haubenreisser, K. Higashigaito, H. Alkadhi, J. N. Morelli, B. Alber, S. O. Schoenberg, and T. Henzler, "Combined static and dynamic computed tomography angiography of peripheral artery occlusive disease: Comparison with magnetic resonance angiography," *CardioVascular Interventional Radiol.*, vol. 41, no. 8, pp. 1205–1213, Aug. 2018.

[8] J. A. Mustapha, L. J. Diaz-Sandoval, and F. Saab, "Infrapopliteal calcification patterns in critical limb ischemia: Diagnostic, pathologic and therapeutic implications in the search for the endovascular holy grail," *J. Cardiovascular Surg.*, vol. 58, no. 3, pp. 383–401, Jun. 2017.

[9] G. Soulez, E. Therasse, M.-F. Giroux, L. Bouchard, P. Gilbert, P. Perreault, G. Cloutier, and V. L. Oliva, "Management of peripheral arterial disease: Role of computed tomography angiography and magnetic resonance angiography," *La Presse Médicale*, vol. 40, no. 9, pp. e437–e452, Sep. 2011.

[10] W. H. Sommer, A. Helck, F. Bamberg, E. Albrecht, C. R. Becker, R. Weidenhagen, H. Kramer, M. F. Reiser, and K. Nikolaou, "Diagnostic value of time-resolved CT angiography for the lower leg," *Eur. Radiol.*, vol. 20, no. 12, pp. 2876–2881, Dec. 2010.

[11] H. Haubenreisser, A. Bigdeli, M. Meyer, T. Kremer, T. Riester, U. Kneser, S. O. Schoenberg, and T. Henzler, "From 3D to 4D: Integration of temporal information into CT angiography studies," *Eur. J. Radiol.*, vol. 84, no. 12, pp. 2421–2424, Dec. 2015.

[12] W. H. Sommer, F. Bamberg, T. Johnson, R. Weidenhagen, M. Notohamiprodjo, F. Schwarz, M. Reiser, and K. Nikolaou, "Diagnostic accuracy of dynamic computed tomographic angiographic of the lower leg in patients with critical limb ischemia," *Investigative Radiol.*, vol. 47, no. 6, pp. 325–331, Jun. 2012.

[13] H.-P. Müller, F. Raudies, A. Unrath, H. Neumann, A. C. Ludolph, and J. Kassubek, "Quantification of human body fat tissue percentage by MRI," *NMR Biomed.*, vol. 24, no. 1, pp. 17–24, Jan. 2011.

[14] K. Popuri, D. Cobzas, N. Esfandiari, V. Baracos, and M. Jägersand, "Body composition assessment in axial CT images using FEM-based automatic segmentation of skeletal muscle," *IEEE Trans. Med. Imag.*, vol. 35, no. 2, pp. 512–520, Feb. 2016.

[15] M. Gadermayr, K. Li, M. Müller, D. Truhn, N. Krämer, D. Merhof, and B. Gess, "Domain-specific data augmentation for segmenting MR images of fatty infiltrated human thighs with neural networks," *J. Magn. Reson. Imag.*, vol. 49, no. 6, pp. 1676–1683, Jun. 2019.

[16] S. Andrews, G. Hamarneh, A. Yazdanpanah, B. HajGhanbari, and W. D. Reid, "Probabilistic multi-shape segmentation of knee extensor and flexor muscles," in *Medical Image Computing and Computer-Assisted Intervention*, vol. 14. Berlin, Germany: Springer, 2011, pp. 651–658.

[17] S. R. Kannan, R. Devi, S. Ramathilagam, and K. Takezawa, "Effective FCM noise clustering algorithms in medical images," *Comput. Biol. Med.*, vol. 43, no. 2, pp. 73–83, Feb. 2013.

[18] A. M. Anter and A. E. Hassenian, "CT liver tumor segmentation hybrid approach using neutrosophic sets, fast fuzzy c-means and adaptive watershed algorithm," *Artif. Intell. Med.*, vol. 97, pp. 105–117, Jun. 2019.

[19] I. Gatos, S. Tsantis, M. Karamesini, S. Spiliopoulos, D. Karnabatidis, J. D. Hazle, and G. C. Kagadis, "Focal liver lesions segmentation and classification in nonenhanced T2-weighted MRI," *Med. Phys.*, vol. 44, no. 7, pp. 3695–3705, Jul. 2017.

[20] P. Saiviroonporn, P. Korpraphong, V. Viprakasit, and R. Krittayaphong, "An automated segmentation of R2* iron-overloaded liver images using a fuzzy C-mean clustering scheme," *J. Comput. Assist. Tomogr.*, vol. 42, no. 3, pp. 387–398, May/Jun. 2018.

[21] P. R. Meena and S. K. R. Shantha, "Spatial fuzzy C means and expectation maximization algorithms with bias correction for segmentation of MR brain images," *J. Med. Syst.*, vol. 41, no. 1, p. 15, 2017.

[22] Y. Wen, L. He, K. M. von Deneen, and Y. Lu, "Brain tissue classification based on DTI using an improved fuzzy C-means algorithm with spatial constraints," *Magn. Reson. Imag.*, vol. 31, no. 9, pp. 1623–1630, Nov. 2013.

[23] Y. Feng, F. Dong, X. Xia, C.-H. Hu, Q. Fan, Y. Hu, M. Gao, and S. Mutic, "An adaptive fuzzy C-means method utilizing neighboring information for breast tumor segmentation in ultrasound images," *Med. Phys.*, vol. 44, no. 7, pp. 3752–3760, Jul. 2017.

[24] T. Gaber, G. Ismail, A. Anter, M. Soliman, M. Ali, N. Semary, A. E. Hassanien, and V. Snasel, "Thermogram breast cancer prediction approach based on neutrosophic sets and fuzzy c-means algorithm," in *Proc. 37th Annu. Int. Conf. IEEE Eng. Med. Biol. Soc. (EMBC)*, Aug. 2015, pp. 4254–4257.

[25] W. Chen, M. L. Giger, U. Bick, and G. M. Newstead, "Automatic identification and classification of characteristic kinetic curves of breast lesions on DCE-MRI," *Med. Phys.*, vol. 33, no. 8, pp. 2878–2887, Aug. 2006.

[26] M.-C. Lee, K.-S. Chuang, M.-K. Chen, C.-K. Liu, K.-W. Lee, H.-Y. Tsai, and H.-H. Lin, "Fuzzy C-means clustering of magnetic resonance imaging on apparent diffusion coefficient maps for predicting nodal metastasis in head and neck cancer," *Brit. J. Radiol.*, vol. 89, no. 1063, Jul. 2016, Art. no. 20150059.

[27] S. T. Schindera, C. Nauer, R. Treier, P. Trueb, G. von Allmen, P. Vock, and Z. Szucs-Farkas, "Strategien zur reduktion der CT-strahlendosis," (in Germany), *Der Radiologe*, vol. 50, no. 12, pp. 1120–1127, Dec. 2010.

[28] D. Zhang, Y. Xie, H. Xue, X. Wang, and Z. Jin, "Feasibility of peripheral artery CT angiography under 70 kV with 50 ml contrast medium on the third-generation dual-source CT," *Zhongguo Yi Xue Ke Xue Yuan Xue Bao*, vol. 39, no. 1, pp. 107–113, Feb. 2017.

[29] B. Horehledova, C. Mihl, G. Milanese, R. Brans, N. G. Eijsvoogel, B. M. F. Hendriks, J. E. Wildberger, and M. Das, "CT angiography in the lower extremity peripheral artery disease feasibility of an ultra-low volume contrast media protocol," *CardioVascular Interventional Radiol.*, vol. 41, no. 11, pp. 1751–1764, Nov. 2018.

[30] N. Saltybaeva, M. E. Jafari, M. Hupfer, and W. A. Kalender, "Estimates of effective dose for CT scans of the lower extremities," *Radiology*, vol. 273, no. 1, pp. 153–159, Jun. 2014.

[31] M. C. Stoner, K. D. Calligaro, Rabih A. Chaer, Alan M. Dietzek, A. Farber, R. J. Guzman, A. D. Hamdan, G. J. Landry, and D. J. Yamaguchi, "Reporting standards of the society for vascular surgery for endovascular treatment of chronic lower extremity peripheral artery disease," *J. Vascular Surg.*, vol. 64, no. 1, pp. e1–e21, Jul. 2016.

[32] L. Qi, Y. Zhao, C. S. Zhou, J. V. Spearman, M. Renker, U. J. Schoepf, L. J. Zhang, and G. M. Lu, "Image quality and radiation dose of lower extremity CT angiography at 70 kVp on an integrated circuit detector dual-source computed tomography," *Acta Radiolog.*, vol. 56, no. 6, pp. 659–665, Jun. 2015.

[33] M. M. McDermott, "Lower extremity manifestations of peripheral artery disease: The pathophysiologic and functional implications of leg ischemia," *Circulat. Res.*, vol. 116, no. 9, pp. 1540–1550, Apr. 2015.

[34] D. A. Duprez, M. M. De Buyzere, L. De Bruyne, D. L. Clement, and J. N. Cohn, "Small and large artery elasticity indices in peripheral arterial occlusive disease (PAOD)," *Vascular Med.*, vol. 6, no. 4, pp. 211–214, Nov. 2001.
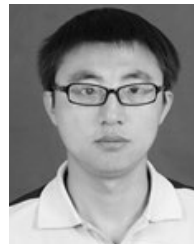
ZEHONG LIN was born in 1981. He received the B.S. degree in mechanical and electronic engineering from the Lanzhou University of Technology, Lanzhou, China, in 2009, and the master's degree in mechanical engineering from Jiamusi University, Jiamusi, China, in 2004, and is currently pursuing the Ph.D. degree with Harbin Engineering University. His research interests include autonomous robot, biomedical robotics, and computer applications.

HE XU was born in 1964. He received the B.S. degree in fluid transmission and pressure control from Zhejiang University, Hangzhou, China, in 1987, and the M.Sc. and Ph.D. degrees in mechatronic control and automation from the Harbin Institute of Technology, Harbin, China, in 1990 and 2006, respectively. He has participated in several national and metro projects in the Middle East. He is currently a Professor with Harbin Engineering University and the Director of the HEU-DYNAVIO Joint Laboratory. He has published more than 40 refereed articles in technical journals and conference proceedings. His research interests include special robots in extreme conditions, design and manufacturing for advanced hydraulic fluid systems, big data mine of manufacture process, robotic maintenance equipment for rail transportation, and weak signal processing for integrated device and its multiphysics coupling optimization.

DAMING ZHANG was born in 1984. She received the Medical Doctor degree from Peking Union Medical College (PUMC), Beijing, China, in 2011. She has participated in several Chinese national projects. She is currently an Associate Professor with PUMC and an Attender at the Department of Radiology, PUMC Hospital. Her research interests include vascular imaging and lymphatic vessel imaging.

• • •